applied optics

Miniaturized time-resolved Raman spectrometer for planetary science based on a fast single photon avalanche diode detector array

Jordana Blacksberg,[1,*] Erik Alerstam,[1] Yuki Maruyama,[1] Corey J. Cochrane,[1] and George R. Rossman[2]

[1]Jet Propulsion Laboratory, California Institute of Technology, Pasadena, California 91109, USA
[2]California Institute of Technology, Division of Geological and Planetary Sciences, Pasadena, California 91125, USA
*Corresponding author: jordana.blacksberg@jpl.nasa.gov

Received 7 October 2015; revised 11 December 2015; accepted 11 December 2015; posted 15 December 2015 (Doc. ID 251466); published 22 January 2016

We present recent developments in time-resolved Raman spectroscopy instrumentation and measurement techniques for *in situ* planetary surface exploration, leading to improved performance and identification of minerals and organics. The time-resolved Raman spectrometer uses a 532 nm pulsed microchip laser source synchronized with a single photon avalanche diode array to achieve sub-nanosecond time resolution. This instrument can detect Raman spectral signatures from a wide variety of minerals and organics relevant to planetary science while eliminating pervasive background interference caused by fluorescence. We present an overview of the instrument design and operation and demonstrate high signal-to-noise ratio Raman spectra for several relevant samples of sulfates, clays, and polycyclic aromatic hydrocarbons. Finally, we present an instrument design suitable for operation on a rover or lander and discuss future directions that promise great advancement in capability.

OCIS codes: (300.6450) Spectroscopy, Raman; (300.6500) Spectroscopy, time-resolved; (140.3538) Lasers, pulsed; (120.6200) Spectrometers and spectroscopic instrumentation.

http://dx.doi.org/10.1364/AO.55.000739

1. INTRODUCTION

A. Raman Spectroscopy for Planetary Science

Over the past several decades, laser Raman spectroscopy has become an important technique in a wide range of fields, including geology and mineralogy [1,2] pharmaceuticals [3], life sciences [4] and medicine [5], art and archeology [6], gemology [7], and national security [8]. Its wide applicability comes from the fact that each band in a Raman spectrum represents interaction of incident light with a vibrational mode in the molecule or crystal; it is therefore highly material specific and can be used for identification and structural characterization of unknown samples. For planetary science, laser Raman spectroscopy offers an attractive *in situ* method for robotic exploration of planetary surfaces that can combine capabilities for the identification of minerals present in geological materials, with capabilities to detect organic matter [9–14]. Additionally, Raman is a nondestructive technique that requires no sample preparation and is well suited for deployment on a planetary rover or lander. In combination with microscale imaging and point mapping, Raman spectroscopy can be used to directly interrogate rocks and regolith materials, while placing compositional analyses within a microtextural context (e.g., see Fig. 1), essential for understanding surface evolutionary pathways. Due to these unique capabilities, Raman spectroscopy is of great interest for the exploration of all rocky and icy bodies, including Mars, Venus, the Moon, Mars' moons, asteroids, comets, Europa, and Titan.

Raman spectroscopy for space exploration has become a reality with the recent selection of Raman instruments by both NASA and ESA for the upcoming Mars 2020 and ExoMars missions. The Mars 2020 payload will include a remote Laser induced breakdown spectroscopy (LIBS)/Raman instrument (SuperCam) [15] and an arm-mounted ultraviolet (UV) fluorescence and resonance Raman spectrometer (SHERLOC) [16], which is highly specialized to detect specific organic compounds. The Raman Laser Spectrometer (RLS) [17] on ESA's ExoMars Rover is a 532 nm Raman spectrometer that will measure powdered samples brought onboard the rover for analysis.

Although the Raman technique is over 80 years old, it is only now gaining traction for applications requiring miniaturized, robust, low-power instruments. These new applications, which include exploration of the planets as well as field exploration on Earth with handheld Raman spectrometers, are made possible by combined technological advances in the areas of

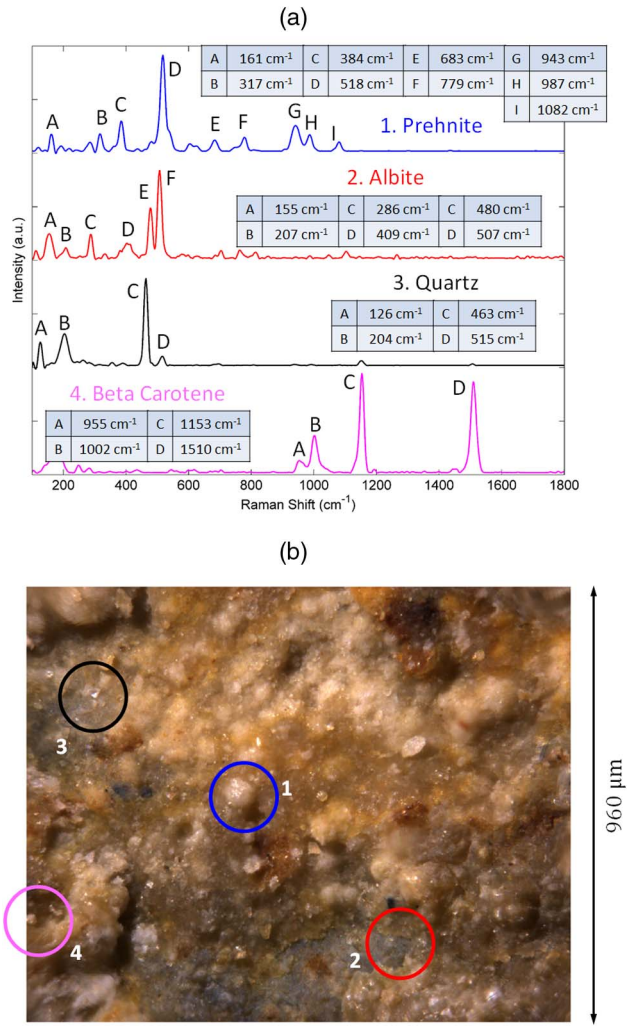

Fig. 1. Time-resolved Raman point map of a shear surface within a basaltic unit of the Miocene age Topanga Canyon Formation, Griffith Park, California. This figure illustrates the ability to combine microtextural information with mineralogy and organics detection. The spectra in (a) correspond to the points in the image (b) which shows a fine-grained "fault gouge" along the shear surface containing isolated mineral grains (1–4 and associated spectra), within a fine matrix. The exposed, weathered surface was colonized by endolithic microorganisms, indicated by beta carotene in spectrum four.

lasers, detectors, optical system design, and computer control and analysis.

In this work we demonstrate how these technological advances, especially in the areas of pulsed lasers and time-resolved detectors, can be applied to Raman spectroscopy in order to achieve improved performance of the Raman technique. We present an overview of Raman spectroscopy, specifically as it applies to *in situ* analysis of planetary surface materials in their natural state, which often includes high fluorescence background. We then discuss instrument architecture with a focus on the key enabling technologies—pulsed microchip lasers and time-resolved single photon avalanche diode (SPAD) detector arrays. Next, we present results obtained on planetary surface analog samples, demonstrating the improved performance made possible by the time-resolved technique. We show an example architecture demonstrating the feasibility of miniaturizing a time-resolved Raman instrument that would be suitable for operation on a rover arm. Finally, we discuss future directions that could lead to further advances.

B. Background Interference

Raman scattering is a weak phenomenon, and therefore the presence of background light can significantly degrade the signal-to-noise ratio (SNR) of Raman spectra. The primary sources of background light are ambient light and fluorescence from the sample itself, induced by the Raman laser probe.

The standard technique for eliminating ambient light from Raman spectra involves significant spectrometer baffling as well as sample shielding enclosures. In laboratory spectrometers, the optical path, including the sample, is typically inside of a dark enclosure. In field portable *in situ* instruments, complete enclosure is difficult to achieve, and ambient light can contribute to the background.

Across all fields in which Raman is applied, the background present from laser-induced sample fluorescence is cited as perhaps the greatest challenge. Even the presence of trace impurities and organics in a sample that is otherwise nonfluorescent can produce strong fluorescence that interferes with the ability to identify the materials present. For geological samples there are two significant sources of fluorescence: fluorescence from the minerals themselves (due to, e.g., impurities or defects in the mineral crystal lattice) or from organic molecules present in the sampling volume. The two types of fluorescence differ in their time scales, with mineral fluorescence typically of the order of hundreds of nanoseconds (ns) to milliseconds (ms) [18]. Organics, on the other hand, fluoresce on shorter time scales in the sub-nanosecond to nanosecond range [19].

Several approaches have been explored in order to mitigate the well-known fluorescence problem [20]. The following Section 1.C summarizes the main approaches that have been used to optimize SNR while at the same time minimizing background interference. These methods rely mainly on selection of an advantageous source wavelength or shifted excitation methods using multiple wavelengths. We then highlight the advantages of using time resolution for this purpose in Section 1.D.

C. Source Wavelength Selection

The selection of an excitation source wavelength for Raman spectroscopy is an important one, with a bearing on the ultimate sensitivity of the technique for the materials of interest. While the intensity of the Raman signal varies as λ^{-4} favoring a short wavelength excitation source (e.g., UV), other factors often come into play which lead to the choice of longer wavelengths such as 532, 785, and 1024 nm. Each has its advantages and disadvantages. UV excitation is the best choice for many organics, which exhibit a large resonance Raman effect [21]. This advantage is compounded by the fact that in the deep UV ($< \sim 250$ nm) the Raman is spectrally well separated from fluorescence, which may occur in these molecules. Longer wavelength UV (e.g., 355 nm) has also been demonstrated [22]. UV Raman (combined with time gating) has been applied to mineralogy using 248, 266, and 355 nm sources, with potential advantages demonstrated for Raman spectroscopy of calcite samples containing multiple luminescence centers [23].

However, since UV light is absorbed in a very thin surface layer of material, when looking at dark materials (e.g., many major rock-forming minerals) the UV Raman return is weak. For such materials, and for mineralogy in general, longer wavelengths in the visible and infrared are preferred. Green excitation sources (e.g., 532 nm) are common in laboratory instruments used for geology and materials science. With a green excitation source, most minerals yield strong enough Raman return for spectral identification. However, when excited with green light, many minerals and organics will fluoresce at wavelengths that spectrally overlap with the Raman return, confounding results. One solution to the fluorescence problem is to use an infrared excitation source (e.g., 785 or 1024 nm). This solution is gaining popularity, especially for handheld Raman spectrometers targeting the geosciences. The disadvantage of infrared excitation over green excitation is that the Raman return is significantly weaker leading to lower SNR as well as longer collection times [24]. Additionally, infrared sources can still excite fluorescence in some materials, so the problem is not completely eliminated (e.g., trace amounts of Nd^{3+}, Pr^{3+}, and Er^{3+} can cause intense fluorescence in the infrared).

Recently, shifted excitation methods for extracting Raman information from interfering backgrounds have been gaining widespread use in the laboratory and portable Raman spectrometers using 532 to 785 nm sources, as a means for mitigating fluorescence interference [24–27]. These methods have been applied to a wide variety of samples with great success for dealing with background interference. However, the drawback of these methods is that the fluorescence must be recorded by the detector for accurate subtraction, thereby still contributing to the dominant shot noise. Thus, in the presence of very strong fluorescence, shifted excitation techniques on their own are insufficient.

D. Time-Resolved Raman Technique

1. Overview

In this work we demonstrate the advantages of time-resolved Raman spectroscopy [28,29] using a 532 nm excitation source. This technique offers a means of using a visible light (green) excitation source while at the same time effectively reducing fluorescence interference. An important distinction here is that in time-resolved Raman, fluorescence is not recorded by the detector and so does not contribute to shot noise as it does in other background removal techniques. The technique works by discriminating between Raman and fluorescence in the time domain since each of these processes occurs at different time scales. Raman scattering is virtually instantaneous (<1 ps) while fluorescence lifetimes vary from ps to ms time scales depending on the material. In addition to eliminating fluorescence, time-resolved spectroscopy offers the important operational advantage of excluding ambient light (which is a continuous source and easily eliminated using this technique). This means that the instrument can operate in daylight either in the field or on a planetary surface mission without the need for light shielding.

An illustration of how time-resolved Raman works is shown in Fig. 2. A pulsed laser is used as an excitation source, and a time-gated detector is synchronized with the pulsed laser. The detector gate is "on"—i.e., the detector is recording

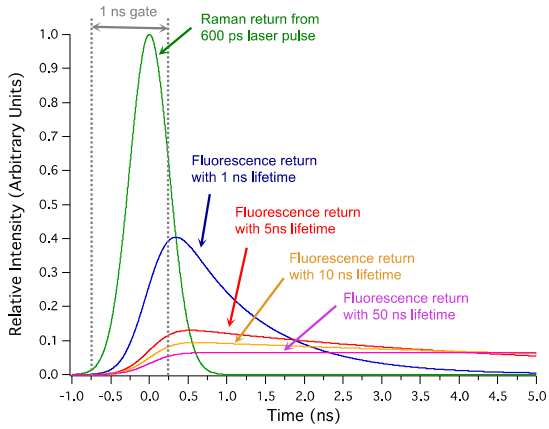

Fig. 2. Illustration of time evolution of Raman and fluorescence shown for a 600 ps laser pulse. The green curve represents the Raman return. The blue, red, orange, and magenta curves represent the return from fluorescence with different lifetimes, convolved with the laser pulse. The 1 ns time gate (the time window where the detector is on) is activated prior to the laser pulse. The time resolution achievable in the case of this ideal gate is approximately equal to the laser pulse duration. As shown, gating rejects a significant portion of the fluorescence and is most effective when the fluorescence lifetime is longer than the time gate.

signal—only during the Raman return, which occurs instantaneously. The fluorescence, which has a longer lifetime, is not collected as it occurs outside of the gate. It is evident from this example that the lifetime of the fluorescence will determine how short the laser pulse and gate must be to effectively reject fluorescence. An added feature of the time-gate technique is that it is possible to scan the gate in time and measure fluorescence lifetime. In this way, we can distinguish between short and long lifetime fluorescence. In planetary science, this could be very useful as a means to detect the presence of organics with short lifetimes, even if they are present in concentrations far below the Raman detection limit.

2. Enabling Technology

We have previously demonstrated the potential value of time-resolved Raman spectroscopy for planetary science by showing significant fluorescence rejection on geological samples using this technique [30]. At the time, the state-of-the-art and most promising hardware for performing time-resolved spectroscopy on the sub-ns time scale used a streak camera as a detector synchronized with a pulsed microchip laser source. While streak cameras are somewhat complex and difficult to miniaturize, at the time of that work no suitable alternative solid-state detector array existed that was capable of sub-ns time resolution while at the same time satisfying the stringent requirements for Raman spectroscopy. Over the past few years, this notion has rapidly changed with the development of single photon avalanche diode arrays, which operate in the single photon counting mode with entirely digital output. SPADs are capable of sub-ns time gating, using very little power, and operating without the need for cooling over a wide temperature range. As such, we quickly concluded that SPADs would represent the enabling technology for time-resolved Raman in a miniaturized

format [31]. Indeed, with recent technological advancements, the use of SPAD detectors for time-resolved Raman spectroscopy is gaining attention in the broader community [32].

Along with the time-resolved detector, the characteristics of the pulsed laser are critical in determining the ultimate time resolution and SNR performance of the time-resolved Raman technique. Passively *Q*-switched diode-pumped solid-state (DPSS) microchip lasers are the technology of choice for this application because they offer performance and reliability in a compact, robust package suitable for space flight applications. Although not with the specifications required here, several similar DPSS lasers have been qualified and flown on NASA missions, for example, the LIDAR instrument on the Mars Phoenix Scout mission [33].

It is these recent advances in solid-state time-resolved detectors and pulsed lasers described above that now make it feasible to implement time-resolved Raman spectroscopy on a rover or lander with little added complexity, size, weight, or power when compared to a conventional continuous wave (CW) Raman spectrometer. It is the combination of this miniaturization with the promise of greatly improved capability that motivates this work.

2. EXPERIMENTAL

A. Instrument Overview

A schematic of the time-resolved Raman spectrometer used in this work is shown in Fig. 3. It is a laboratory benchtop instrument prototype that uses subsystem components that are suitable for space flight (or have alternatives which are readily available that are suitable for space flight).

To acquire time-resolved Raman spectra, a 532 nm passively *Q*-switched pulsed microchip laser (TEEM Photonics SNG MicroChip) delivers ~1.5 μJ, ~600 ps, spectrally narrow (<0.1 nm) pulses at a repetition rate of 40 kHz. A small portion of the beam is sampled and delivered to a trigger photodiode, which synchronizes the pulse arrival with the SPAD detector gating. The main laser beam is attenuated to a power level appropriate for the sample using standard ND filters and delivered to the sample through a 0.60 NA microscope objective (Qioptic, Optem 20X M Plan APO LWD). The laser spot is defocused slightly to reduce the power density on the sample. In this work the laser was intentionally defocused to provide an ~5 μm spot size on the sample. The return light is delivered to a spectrometer through a dichroic edge filter (Semrock 532 nm RazorEdge ultrasteep long-pass edge filter). A fiber delay line consisting of a 10 m long graded index fiber (Thorlabs GIF625) is used to ensure that there is sufficient time for the SPAD to trigger before the return light reaches the detector. The spectrometer used in this work is a standard commercial transmission grating spectrometer (Kaiser Optical HoloSpec f/1.8i VIS with a HSG-532-LF grating), providing a –50–2200 cm^{-1} spectral range and ~6 cm^{-1} spectral resolution. With the use of a beam splitter, a microscopic imager records images of the sample through the same objective lens, allowing for imaging of the laser spot on the sample. A three-axis translation stage is used for sample positioning, and focus stacking (a standard procedure used to extend depth of field [34]) is used to obtain focused images over the entire image area for real mineral samples with unprepared surfaces and high roughness.

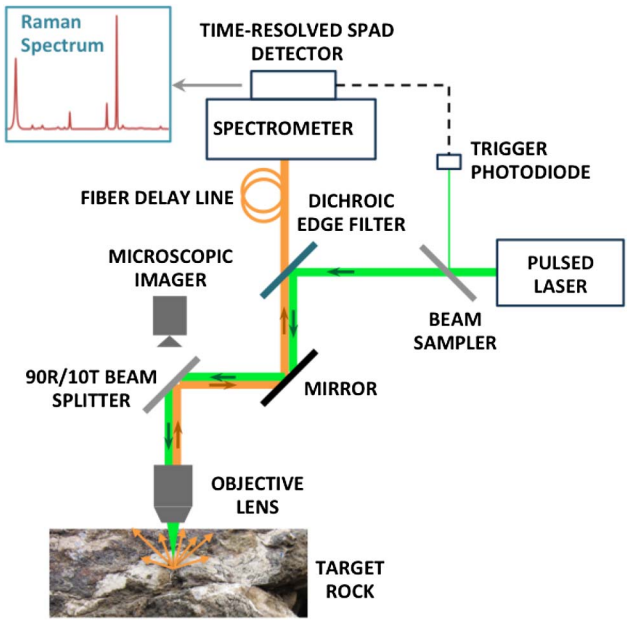

Fig. 3. Schematic of the time-resolved Raman spectrometer.

B. Time-Resolved Detector

In this work we use a 1024 × 8 pixel SPAD array described in detail by Maruyama *et al.* [35] and shown in Fig. 4. This SPAD array was designed and fabricated using standard CMOS processes that have been used for many other flight components and are therefore compatible with space flight applications that we are targeting here. The rise and fall times of the gate are 550 ps and 250 ps, respectively. The gate width is adjustable, but in practice the optimal gate width is chosen to be as short as possible given the limitations imposed by the laser pulse width and gate fall time. This is determined experimentally by optimizing Raman SNR as the gate width is varied. Using this method, an ~1 ns gate was chosen for this work.

C. Measurement Procedure and Calibration

In order to convert spectroscopic data collected with the SPAD array to useful Raman spectra, several calibrations are required. First, prior to each measurement a dark spectrum is acquired which is later subtracted from the acquired spectrum. Second,

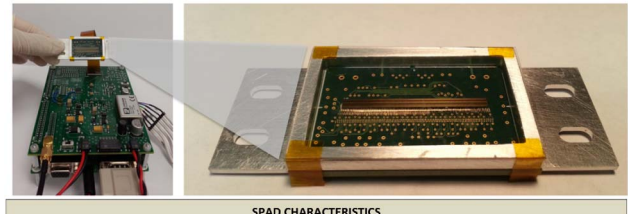

SPAD CHARACTERISTICS	
• 8 x 1024 array of SPADs	• Pixel includes SPAD, gating circuit, 1 bit counter
• 700 ps minimum gate width	• 250 ps on-chip delay line
• 1.2 mm² x 24.7 mm² chip size	• Sensitivity: > 20%
• 24 μm² x 24 μm² detector pitch	• Noise: 7.4 kHz
• 16.8 μm² x 15.7 μm² detector active area (44%)	

Fig. 4. (left) Custom 1024 × 8 SPAD array integrated with FPGA and power module, and (right) close-up of the SPAD array.

the wavenumber must be calibrated. This is accomplished using a standard sample with known Raman peaks. In this work cyclohexane is used. Third, a relative intensity calibration is performed to compensate for the variations in spectral throughput of the instrument, detector sensitivity, etc. This is accomplished using a spectrally calibrated broadband lamp (Thorlabs SLS201). After applying the dark noise correction, wavenumber calibration, and relative intensity calibration, the data are in their final usable form.

Additional post-processing can be used to subtract any remaining baseline that is present from short lifetime fluorescence that is not completely rejected by time gating. Finally, the determination of mineral phases present from the measured spectra is accomplished with the use of our custom classification software [36] designed to handle large databases with robustness against inconsistencies in database spectra related to, for example, variability in instrumentation and sample purity. In this work we use the RRUFF (RRUFFÔ Project: http://rruff.info/) database combined with our own database of collected spectra to determine the mineral phases present in mixtures such as naturally occurring rock samples.

3. RESULTS

A. Time-Resolved Raman Measurements of Minerals Relevant to Planetary Science

We have performed time-resolved Raman measurements on a wide range of natural geological samples containing both minerals and organics, many of which are highly relevant to planetary science investigations. For example, on Mars it is now well understood that habitable environments once existed in places like Gale Crater [37]. Minerals associated with sedimentary deposits and aqueous alteration, such as clays and sulfates, have been identified in these environments on Mars from both orbit and *in situ* [38–41]. Future missions could be aimed at seeking samples for return to Earth, potentially from similar habitable environments that are most likely to contain evidence of past life [42,43]. By analogy, many aqueously formed minerals from similar environments on Earth show high levels of background fluorescence [44–46]. In the search for fossilized organic matter on Mars, time-resolved Raman spectroscopy would therefore be a highly capable method for characterizing the surface mineralogy under a wide range of conditions including a high fluorescence background. In this section, we demonstrate the capabilities of the technique by showing time-resolved Raman spectra for several challenging natural mineral samples.

1. Sulfate Minerals

Most sulfate minerals require an aqueous environment for their formation and are thus of great interest in elucidating planetary geologic histories, for example, on Mars. Since many clays and sulfates form under different conditions (e.g., clays typically require a neutral pH while many sulfates require acidic conditions), the existence of both of these types of minerals in different layers in the same location can indicate the changing conditions at that site and can place constraints on the time frames where habitable conditions prevailed [47,37]. Magnesium sulfate is one such mineral that has been identified on the surface of Mars from orbit. It is hygroscopic and can exist in a number of different hydration states, depending on its environmental history. Raman spectroscopy is an excellent method for identification of magnesium sulfate minerals, and the peak positions can provide additional information about the hydration state, with peaks shifting to higher wavenumber with decreasing hydration [48]. Although magnesium sulfate is not in itself fluorescent, because these minerals form in aqueous environments, they often concentrate impurities (minerals and organics) that are fluorescent when illuminated with a laser. For example, the natural magnesium sulfate sample CIT2222 is highly fluorescent and Raman spectra could not be attained using CW Raman. The time-resolved spectrum of this sample is shown in Fig. 5. In this case, time-resolved Raman spectroscopy yields a high SNR magnesium sulfate spectrum with excellent fluorescence rejection. The peak positions in this spectrum reveal that the sample is hydrated, matching most closely to starkeyite.

2. Clay Minerals

Clay minerals are ubiquitous on Earth and are the end products of weathering of a wide variety of rocks [49]. Clays are of prime importance to life on Earth as they play a fundamental role in the properties of soil. Many clays such as montmorillonite favor neutral pH conditions as well and can thus serve as an indicator for the presence or history of aqueous conditions favorable to life on other planets. Despite their importance, clays present a number of distinct challenges to mineralogical characterization. They are fine-grained with large variability in chemical composition and are rarely found in pure form but rather mixed with other fine-grained minerals. Raman spectroscopy of clays is notably challenging due to the fine grains size, the weak polarizability of the Si—O and Si═O in the clay structure, coupled with frequent high fluorescence background interference. To combat fluorescence, FT-Raman is frequently used in the laboratory [50,51,44] where high laser power and long scans can be used to achieve acceptable SNR.

Figure 6 shows a time-resolved Raman spectrum of a montmorillonite clay sample (H-19) from Polkville, Mississippi. This sample exhibited extremely high background fluorescence in a conventional CW Raman spectrometer, preventing the Raman peaks from being distinguished. Using time-resolved Raman, we were able to distinguish four different minerals

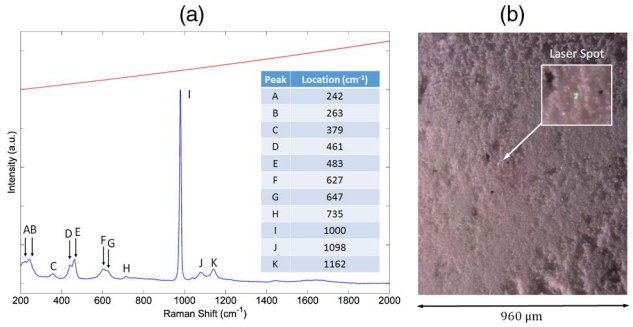

Fig. 5. (a) Time-resolved Raman spectrum (not baseline corrected) of a highly fluorescent natural magnesium sulfate sample CIT 2222. This sample could not be characterized using CW Raman due to extremely high fluorescence that saturated the CCD detector. Time-resolved Raman reveals a hydrated phase with a best match to starkeyite. (b) Microscope image of the laser spot incident on the sample.

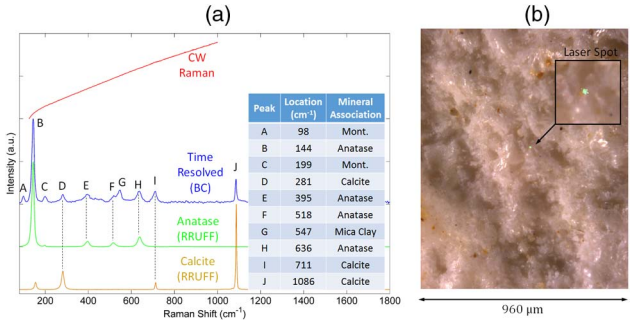

Fig. 6. Time-resolved Raman spectrum (blue) of montmorillonite H-19 from Polkville, Mississippi. This spectrum has been baseline corrected (BC) and shifted vertically for clarity. Peaks labeled "Mont." are attributed to montmorillonite. The presence of two minor phases, calcite and anatase, is apparent in the time-resolved spectrum. A single peak labeled G may be attributed to a green mica clay. Spectra of calcite and anatase from the RRUFF database are shown here in green and light blue. For comparison, a measurement of the same montmorillonite sample on a standard continuous-wave Raman spectrometer (without time-resolution) is shown in red. This spectrum was acquired over 1 s. Longer acquisition time quickly saturated the CCD detector due to extremely high fluorescence background. As a result, no spectral features could be distinguished without the use of time resolution.

in this sample: montmorillonite, anatase, calcite, and a possible green mica clay [52].

While many clay samples exhibit very strong fluorescence similar to what was observed in the montmorillonite H-19 sample, some clay samples exhibit moderate fluorescence where CW measurements can provide some useful data, though such data can sometimes be inconclusive. In such samples, the use of time resolution can improve the SNR of the measured spectra appreciably. An example is shown in Fig. 7 using hectorite, a lithium-containing smectite clay. This sample exhibited moderate fluorescence as can be observed in the sloping background of the CW spectrum. With the use of time gating, the fluorescence background is appreciably reduced but can still be observed. It can be concluded that the lifetime of the responsible fluorophor is of the order of several nanoseconds, and therefore the 1 ns time gate only rejects a portion of the fluorescence background.

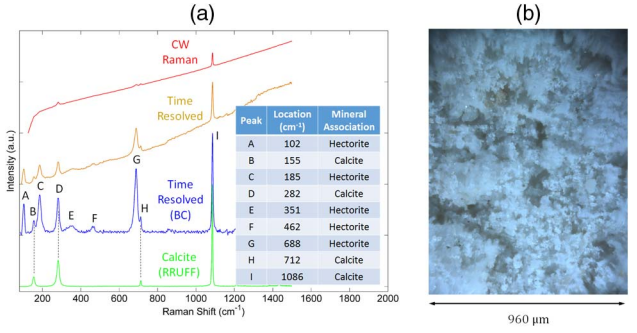

Fig. 7. Time-resolved Raman spectrum of hectorite from Hector, California (Wards) shown in gold, with the same spectrum shown after baseline correction (BC) in blue. In addition to hectorite, a minor phase of calcite is observed and can be compared to the calcite Raman spectrum from the RRUFF database shown in green. For comparison to CW Raman (without time resolution), both the CW and time-resolved spectra are shown on the same normalized scale, without baseline subtraction (red and gold, respectively). It is clear from this data that the fluorescence background is significantly reduced by time gating, although not completely eliminated.

B. Time-Resolved Raman Measurements of Organics

The presence of fluorescence originating from organics is of concern for nearly all planetary bodies and is expected to be highly variable throughout the solar system. Here we consider polycyclic aromatic hydrocarbons (PAHs) compounds that are ubiquitous throughout the solar system and can be strongly fluorescent [53]. On Earth, PAHs are the products of transformation of buried primary organic matter, forming geopolymers like kerogen as the result of biodegradation processes. A similar process is thought to have been possible on Mars, where habitable environments are known to have existed. In addition, PAHs have been reported in carbonaceous chondrite meteorites, Martian meteorites, stardust comet samples, interplanetary dust particles, and interstellar matter. PAHs have also been identified spectroscopically on the surface of Saturn's moon Titan, [54] an organic-rich body where fluorescence is expected to be significant. In light of the diverse occurrences of PAHs, a method for their reliable detection and characterization is desired for a wide range of applications, one of which is determining the potential for habitability and life elsewhere in the solar system.

Coronene is a PAH with the chemical formula $C_{24}H_{12}$ and is one of the many organic compounds that has been identified spectroscopically on Titan [54]. It can also be found in nature as the mineral carpathite. In this work we have measured Raman spectra from a synthetic coronene sample containing trace impurities and exhibiting a very high fluorescence background when excited with the laser. This sample could not be characterized by CW Raman spectroscopy due to overwhelming fluorescence. Time-resolved Raman spectra for this sample are shown in Fig. 8. Spectra are shown for our standard 1 ns gate, as well as for a 16 ns gate intended to emulate a CW-like measurement (i.e., the gate is left open after the Raman process is complete at which point fluorescence continues to be detected). It is clear from the high background and the absence of Raman spectral features that a time gate of 16 ns is insufficient to gate out the relatively short lifetime fluorescence in this sample. With the 1 ns gate, fluorescence is partially rejected, and three coronene peaks are visible.

4. DISCUSSION

A. Feasibility for Planetary Surface Applications

With planetary science applications in mind, a major goal of our work is to miniaturize the time-resolved instrument and package it in a way that is suitable for use on a planetary lander or rover. Such a compact design could also be adapted more generally to operation as a handheld instrument either by astronauts or field geologists on Earth. The suitability for miniaturization has been a driving factor for all components chosen for this work and most specifically the laser and detector which are highly miniaturizable when compared to other technologies that are limited to use in laboratory studies (e.g., Ti:sapphire lasers, streak cameras). Furthermore, when choosing our

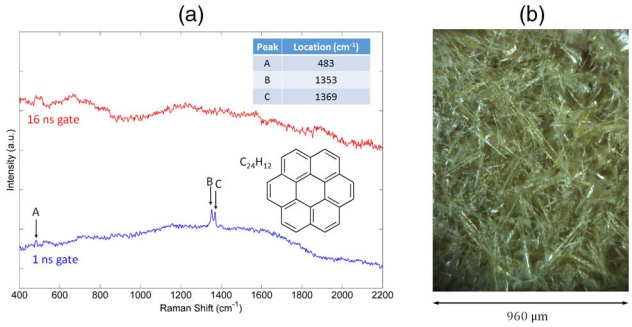

Fig. 8. Time-resolved Raman spectra for a coronene sample containing trace impurities responsible for the extremely high fluorescence background. A 16 ns gate is not short enough to reduce the fluorescence background to a level where Raman spectra can be obtained. With a 1 ns gate, a Raman spectrum emerges and three coronene Raman peaks can be detected. However, improved time resolution would be desirable for achieving better signal-to-noise spectra.

subsystem components with space applications in mind, we have paid attention to size, weight, and power consumption, as well as robustness to vibration and radiation. It is important to note that although we work with nonflight parts in this laboratory prototype, all components used in this work can potentially be designed to meet the necessary requirements.

As a demonstration of the feasibility of miniaturization for space applications, we present here a model of a time-resolved Raman instrument designed for operation on a Mars rover arm shown in Fig. 9. The arm-mounted instrument contains the following modules: an optical bench for co-aligned Raman and imaging, a pulsed laser source, two miniature spectrometers with custom nanosecond time-gated detectors, and an electronics module. To the extent possible, all electro-opto-mechanical components required for time-resolved Raman measurements are accommodated within the arm-mounted unit and are optically connected using stationary short (standard step index multimode) optical fibers, fully enclosed in the instrument. This modular design strategy allows for relatively independent development of the modules, using flight heritage components where possible. Though we have chosen a specific arm-mounted architecture here, the exact placement of these modules is flexible, enabling straightforward adaptation to a broad range of missions with differing requirements. The estimated mass for the arm-mounted module is 1.8 kg (the total mass including body-mounted components would be ~2.5 kg). The power consumption is estimated at a peak power of <10 W and a typical operating power during Raman measurement of ~6 W. The two spectrometers are designed to cover the two primary regions of interest in Raman spectroscopy of minerals and organics: ~100– ~ 1800 cm^{-1} (spectrometer 1) and ~1800– ~ 4000 cm^{-1} (spectrometer 2) keeping the resolution of both spectrometers <10 cm^{-1} over the entire range. While the experiments performed in this work are limited to roughly the range of spectrometer 1, spectrometer 2 is also needed in order to directly probe OH and H_2O vibrational modes, important for hydrated minerals such as the clays and hydrated sulfates discussed in this work. Also of interest, this range would capture N-H stretching modes and C-H stretching modes of

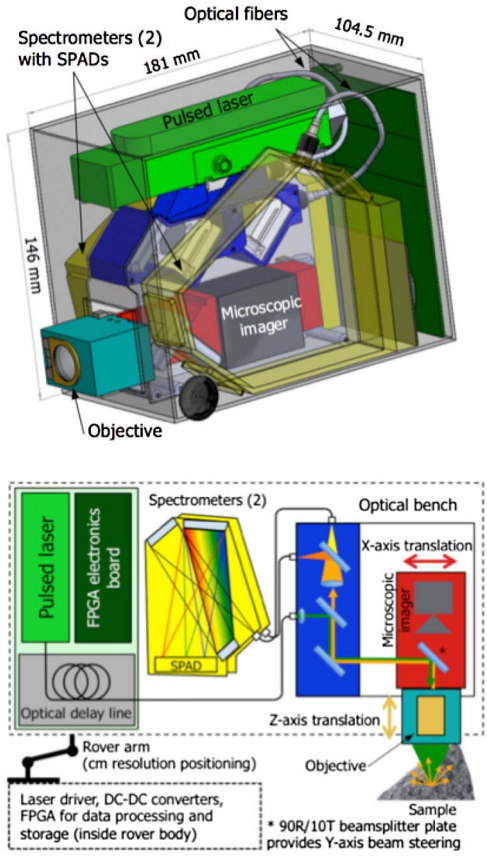

Fig. 9. (top) CAD drawing and (bottom) block diagram of the arm-mounted time-resolved Raman instrument. Components are color-coded for easy identification across both figures. The instrument case measures 144 mm × 181 mm × 104.5 mm and the objective protrudes an additional 29 mm. For scale, a 14 mm diameter U.S. quarter is rendered in the lower left corner of the instrument.

aliphatic and aromatic organic compounds [55]. These miniature spectrometers ($f/4$, crossed Czerny–Turner design) are based on flight heritage spectrometers (e.g., LCROSS, LADEE, O/OREOS, and MSL [56]), with minor modifications.

B. Future Directions

We have demonstrated the effectiveness of time-resolved Raman spectroscopy in reducing fluorescence originating from minerals as well as many organics relevant to geologic samples. However, limitations still exist, particularly for applications where organics are the primary target and where sub-ns lifetime fluorescence dominates. We identify two areas where significant improvements can be made: reducing the effective gate duration for the improved rejection of short lifetime fluorescence and improving the management of the laser power delivered to the sample.

While the SPAD gate width in this work was set to ~1 ns, the minimum practical gate width of the SPAD, which determines the time resolution achievable with this chip, is essentially determined by the rise and fall time of the gate if the laser pulse duration can be made arbitrarily short (see Fig. 10). In theory, if the gate could turn on and off instantaneously then the minimum time resolution would be defined by the laser

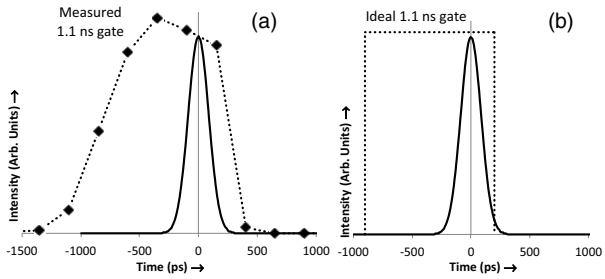

Fig. 10. Simulated laser pulse (solid line) shown with (a) measured 1.1 ns gate (dashed line) displaying 0.55 ns rise and 0.25 ns fall time and (b) an ideal gate with sharp rise and fall. Using an early gating scheme where the gate is activated prior to the laser pulse, the time resolution achievable in the case of the ideal gate is approximately equal to the laser pulse duration (200 ps is used here for illustration).

pulse duration alone. In such a case, the gate would be turned on prior to the laser pulse and turned off precisely at the end of the laser pulse, as illustrated in Fig. 10(b). However, in reality, the measured rise and fall times of the gate are finite. With the SPAD used in this work, we estimate that we would see a significant improvement in fluorescence rejection capability by moving to laser source pulses down to ~100 ps.

Since the time-resolved Raman technique requires the use of a fast pulsed laser, an additional consideration (compared to CW Raman) is required in order to avoid sample damage: minimizing the peak power incident on the sample. From this point of view, a larger laser spot is desirable, but in microscopic Raman spectroscopy, a small spot size is necessary for achieving high spatial resolution and for unambiguous analysis and identification of fine-grained materials. Instead, a better way to reduce the peak power density is to lower the pulse energy and increase the laser repetition rate. This strategy allows for higher average power to be used, improving SNR for samples that are easily damaged by high peak power (e.g., dark samples and sensitive organics).

In this work we have chosen the highest repetition rate laser available commercially which meets all of the other requirements for pulsed Raman in a miniaturized and robust package. However, recent developments in semiconductor saturable absorber technology have realized a significant leap in passively *Q*-switched DPSS microchip laser technology [57–59]. These new lasers offer the same narrow spectral linewidth and excellent beam quality while operating at much higher repetition rates (megahertz) and at pulse energy levels appropriate for our application and with shorter pulse duration (<100 ps). We are currently integrating these lasers into our time-resolved Raman instrument [60] and will pursue this direction in our future work.

5. CONCLUSIONS

Time-resolved Raman spectroscopy offers an attractive strategy for planetary surface exploration, where a wide variety of minerals and organics can be targeted without interference from background fluorescence or ambient light. We have demonstrated the effectiveness of time-resolved Raman using a benchtop instrument prototype with sub-ns time resolution using two recently developed enabling technologies: a time-resolved SPAD detector array and a miniature pulsed microchip laser operating at 532 nm. It is these enabling technologies that have made it feasible to miniaturize a time-resolved Raman instrument into a small package suitable for a planetary rover or lander. In this work we have presented time-resolved Raman spectra for several planetary analog samples including sulfates, clays, and PAHs. These samples were chosen because they are known to pose challenges in the form of high fluorescence, short-lifetime fluorescence, inherently low Raman return, and/or low sample damage threshold. We have shown that time-resolved Raman can be used to obtain high quality Raman spectra, even for these challenging cases where CW Raman has been unsuccessful. Future work will focus on miniaturizing the instrument into a flight-like configuration as well as expanding the capabilities of this technique by exploring high-speed pulsed lasers that promise significant SNR improvements.

Funding. National Aeronautics and Space Administration (NASA) (104528-811073.02.06.02.25).

Acknowledgment. The research described here was carried out at the Jet Propulsion Laboratory, California Institute of Technology, under a contract with the National Aeronautics and Space Administration (NASA). This work was supported in part by the NASA Planetary Instrument Definition and Development Program (PIDDP). Continuous-wave Raman measurements were performed at the Mineral Spectroscopy Laboratory at the California Institute of Technology. SPAD development was performed at Delft University of Technology by the group of Professor Edoardo Charbon. We would like to acknowledge Professor Jack Farmer at ASU for useful input regarding time-resolved Raman for identification of fossilized organic matter and for geologic interpretations of Griffith Park samples.

REFERENCES

1. W. P. Griffith, "Raman spectroscopy of minerals," Nature **224**, 264–266 (1969).
2. P. F. McMillan, "Raman spectroscopy in mineralogy and geochemistry," Annu. Rev. Earth Planet Sci. **17**, 255–279 (1989).
3. G. Fini, "Applications of Raman spectroscopy to pharmacy," J. Raman Spectrosc. **35**, 335–337 (2004).
4. R. Petry, M. Schmitt, and J. Popp, "Raman spectroscopy–a prospective tool in the life sciences," Chemphyschem **4**, 14–30 (2003).
5. E. B. Hanlon, R. N. Manoharan, T.-W. Koo, K. E. Shafer, J. T. Motz, M. Fitzmaurice, J. R. Kramer, I. Itzkan, R. R. Dasari, and M. S. Feld, "Prospects for *in vivo* Raman spectroscopy," Phys. Med. Biol. **45**, R1–R59 (2000).
6. P. Vandenabeel, H. G. Edwards, and L. Moens, "A decade of Raman spectroscopy in art and archaeology," Chem. Rev. **107**, 675–686 (2007).
7. L. Kiefert and S. Karampelas, "Use of the Raman spectrometer in gemological laboratories: review," Spectrochim. Acta Part A **80**, 119–124 (2011).
8. Y. Fledger, L. Nagli, M. Gaft, and M. Rosenbluh, "Narrow gated Raman and luminescence of explosives," J. Lumin. **129**, 979–983 (2009).
9. P. Gasda, T. E. Acosta-Maeda, P. Lucey, A. K. Misra, S. K. Sharma, and G. J. Taylor, "Next generation laser-based standoff spectroscopy techniques for Mars exploration," Appl. Spectrosc. **69**, 173–192 (2015).

10. S. M. Clegg, R. Wiens, A. K. Misra, S. K. Sharma, J. Lambert, S. Bender, R. Newell, K. Nowak-Lovato, S. Smrekar, M. D. Dyar, and S. Maurice, "Planetary geochemical investigations using Raman and laser-induced breakdown spectroscopy," Appl. Spectrosc. **68**, 925–936 (2014).
11. P. Haenecour, C. Floss, A. Wang, and T. Yada, "Raman spectroscopy of organic matter in Antarctic micrometeorites," Meteorit. Planet. Sci. **49**, A150 (2014).
12. J. J. Freemanm, A. Wang, K. E. Kuebler, B. L. Joliff, and L. A. Haskin, "Characterization of natural feldspars by Raman spectroscopy for future planetary exploration," Can. Miner. **46**, 1477–1500 (2008).
13. I. B. Hutchinson, R. Ingley, H. G. M. Edwards, L. Harris, M. McHugh, C. Malherbe, and J. Parnell, "Raman spectroscopy on Mars: identification of geological and bio-geological signatures in Martian analogues using miniaturized Raman spectrometers," Philos. Trans. A **372**, 20140204 (2014).
14. M. S. Angel, N. R. Gomer, S. K. Sharma, and C. McKay, "Remote Raman spectroscopy for planetary exploration: a review," Appl. Spectrosc. **66**, 137–150 (2012).
15. S. M. Clegg, R. C. Wiens, S. Maurice, O. Gasnault, S. K. Sharma, A. K. Misra, R. Newell, O. Forni, J. Lasue, R. B. Anderson, K. L. Nowak-Lovato, T. Fouchet, S. M. Angel, F. Rull, and J. R. Johnson, and the SuperCam Science Team, "Remote geochemical and mineralogical analysis with supercam for the Mars 2020 rover," Houston, Texas, Lunar and Planetary Institute, Lunar and Planetary Science XLVI, abstract 2781 (2015).
16. L. Beegle, R. Bhartia, L. DeFlores, M. Darrach, R. D. Kidd, W. Abbey, S. Asher, A. Burton, S. Clegg, P. G. Conrad, K. Edgett, B. Ehlmann, F. Langenhorst, M. Fries, W. Hug, K. Nealson, J. Popp, P. Sobron, A. Steele, R. Wiens, and K. Willeford, "SHERLOC: scanning habitable environments with Raman & luminescence for organics & chemicals, an investigation for 2020," in *Proceedings of the 11th International GeoRaman Conference* (2014).
17. F. Rull, S. Maurice, E. Diaz, C. Tato, and A. Pacros, and the RLS Team, "The Raman laser spectrometer (RLS) on the ExoMars 2018 rover mission," Houston, Texas, Lunar and Planetary Institute, Lunar and Planetary Science XLII, abstract 2400 (2011).
18. M. Gaft, R. Reisfeld, and G. Panczer, *Luminescence Spectroscopy of Minerals and Materials* (Springer-Verlag, 2005).
19. B. J. Bozlee, A. K. Misra, S. K. Sharma, and M. Ingram, "Remote Raman and fluorescence studies of mineral samples," Spectrochim. Acta Part A **61**, 2342–2348 (2005).
20. G. Panczer, D. de Ligny, C. Mendoza, M. Gaft, A. M. Seydoux-Guillaume, and X. Wang, "Raman and fluorescence," in *EMU Notes in Mineralogy*, J. Dubessy, M.-C. Caumon, and F. Rull, eds., Vol. **12** of Applications of Raman Spectroscopy to Earth Sciences and Cultural Heritage (European Mineralogical Union, 2012), pp. 61–82.
21. S. Asher and J. Murtaugh, "UV Raman excitation profiles of imidazole, imidazolium, and water," Appl. Spectrosc. **42**, 83–90 (1988).
22. M. Skulinova, C. Lefebvre, P. Sobron, E. Eshelman, M. Daly, J.-F. Gravel, J.-F. Cormierm, F. Chateauneuf, G. Slater, W. Zheng, A. Koujelev, and R. Leveille, "Time-resolved stand-off UV-Raman spectroscopy for planetary exploration," Planet. Space Sci. **92**, 88–100 (2014).
23. M. Gaft and L. Nagli, "Gated Raman spectroscopy: potential for fundamental and applied mineralogy," Eur. J. Mineral. **21**, 33–42 (2009).
24. A. Culka, F. Kosek, P. Drahota, and J. Jehlicka, "Use of miniaturized Raman spectrometer for detection of sulfates of different hydration states–significance for Mars studies," Icarus **243**, 440–453 (2014).
25. A. P. Shreve, N. J. Cherepy, and R. A. Mathies, "Effective rejection of fluorescence interference in Raman spectroscopy using a shifted excitation difference technique," Appl. Spectrosc. **46**, 707–711 (1992).
26. S. T. McCain, R. M. Willett, and D. J. Brady, "Multi-excitation Raman spectroscopy technique for fluorescence rejection," Opt. Express **16**, 10975–10991 (2008).
27. J. B. Cooper, M. Abdelkader, and K. L. Wise, "Sequentially shifted excitation Raman spectroscopy: novel algorithm and instrumentation for fluorescence-free Raman spectroscopy in spectral space," Appl. Spectrosc. **67**, 973–984 (2013).
28. P. Matousek, M. Towrie, A. Stanley, and A. W. Parker, "Efficient rejection of fluorescence from Raman spectra using picosecond Kerr gating," Appl. Spectrosc. **53**, 1485–1489 (1999).
29. H. Hamaguchi and T. L. Gustafson, "Ultrafast time-resolved spontaneous and coherent Raman spectroscopy: the structure and dynamics of photogenerated transient species," Annu. Rev. Phys. Chem. **45**, 593–622 (1994).
30. J. Blacksberg, G. R. Rossman, and A. Gleckler, "Time resolved Raman spectroscopy for *in situ* planetary mineralogy," Appl. Opt. **49**, 4951–4962 (2010).
31. J. Blacksberg, Y. Maruyama, E. Charbon, and G. R. Rossman, "Fast single-photon avalanche diode arrays for laser Raman spectroscopy," Opt. Lett. **36**, 3672–3674 (2011).
32. I. Nissinen, J. Nissinen, P. Keranen, A.-K. Lansman, J. Holma, and J. Kostamovaara, "a 2 × (4) × 128 multitime-gated SPAD line detector for pulsed Raman spectroscopy," IEEE Sens. J. **15**, 1358–1365 (2015).
33. A. I. Carswell, J. F. Hahn, V. I. Podoba, A. Ulitsky, V. Ussyshkin, and D. V. Michelangeli, "LIDAR for Mars atmospheric studies on 2007 scout mission 'Phoenix'," in *22nd International Laser Radar Conference*, Matera, Italy (European Space Agency, 2004), p. 973.
34. K. S. Edgett, R. A. Yingst, M. A. Ravine, M. A. Caplinger, J. Maki, F. T. Ghaemi, J. A. Schaffner, J. F. Bell, I. Laurence, J. Edwards, K. E. Herkenhoff, E. Heydari, L. Kah, M. T. Lemmon, M. E. Minitti, T. S. Olson, T. J. Parker, S. K. Rowland, J. Schieber, R. J. Sullivan, D. Y. Sumner, P. C. Thomas, E. H. Jensen, J. J. Simmonds, A. J. Sengstacken, R. G. Wilson, W. Goetz, and L. J. Edwards, "Curiosity's Mars hand lens imager (MAHLI) investigation," Space Sci. Rev. **170**, 259–317 (2012).
35. Y. Maruyama, J. Blacksberg, and E. Charbon, "A 1024 × 8, 0.7 ns time-gated SPAD line sensor for laser Raman spectroscopy and LIBS in space and rover based planetary exploration," IEEE J. Solid State Circuits **49**, 179–189 (2014).
36. C. J. Cochrane and J. Blacksberg, "A fast classification scheme in Raman spectroscopy for the identification mineralogical mixtures using a large database with correlated predictors," IEEE Trans. Geosci. Remote Sens. **53**, 4259–4274 (2015).
37. J. P. Grotzinger, D. Y. Sumner, L. C. Kah, K. Stack, S. Gupta, L. Edgar, D. Rubin, K. Lewis, J. Schieber, N. Mangold, R. Milliken, P. G. Conrad, D. DesMarais, J. Farmer, K. Siebach, F. Calef III, J. Hurowitz, S. M. McLennan, D. Ming, D. Vaniman, J. Crisp, A. Vasavada, K. S. Edgett, M. Malin, D. Blake, R. Gellert, P. Mahaffy, R. C. Wiens, S. Maurice, J. A. Grant, S. Wilson, R. C. Anderson, L. Beegle, R. Arvidson, B. Hallet, R. S. Sletten, M. Rice, J. Bell III, J. Griffes, B. Ehlmann, R. B. Anderson, T. F. Bristow, W. E. Dietrich, G. Dromart, J. Eigenbrode, A. Fraeman, C. Hardgrove, K. Herkenhoff, L. Jandura, G. Kocurek, S. Lee, L. A. Leshin, R. Leveille, D. Limonadi, J. Maki, S. McCloskey, M. Meyer, M. Minitti, H. Newsom, D. Oehler, A. Okon, M. Palucis, T. Parker, S. Rowland, M. Schmidt, S. Squyres, A. Steele, E. Stolper, R. Summons, A. Treiman, R. Williams, and A. Yingst, and MSL Science Team, "A habitable fluvio-lacustrine environment at Yellowknife Bay, Gale Crater, Mars," Science **343**, 1242777 (2014).
38. S. W. Squyres, J. P. Grotzinger, R. E. Arvidson, J. F. Bell III, W. Calvin, P. R. Christensen, B. C. Clark, J. A. Crisp, W. H. Farrand, K. E. Herkenhoff, J. R. Johnson, G. Klingelhöfer, A. H. Knoll, S. M. McLennan, H. Y. McSween, Jr., R. V. Morris, J. W. Rice, Jr., R. Rieder, and L. A. Soderblom, "*In situ* evidence for an ancient aqueous environment at Meridiani Planum, Mars," Science **306**, 1709–1714 (2004).
39. D. T. Vaniman, D. L. Bish, D. W. Ming, T. F. Bristow, R. V. Morris, D. F. Blake, S. J. Chipera, S. M. Morrison, A. H. Treiman, E. B. Rampe, M. Rice, C. N. Achilles, J. P. Grotzinger, S. M. McLennan, J. Williams, J. F. Bell III, H. E. Newsom, R. T. Downs, S. Maurice, P. Sarrazin, A. S. Yen, J. M. Morookian, J. D. Farmer, K. Stack, R. E. Milliken, B. L. Ehlmann, D. Y. Sumner, G. Berger, J. A. Crisp, J. A. Hurowitz, R. Anderson, D. J. Des, Marais, E. M. Stolper, K. S. Edgett, S. Gupta, and N. Spanovich, and MSL Science Team, "Mineralogy of a mudstone at Yellowknife Bay, Gale Crater, Mars," Science **343**, 1243480 (2014).

40. B. L. Ehlmann, J. F. Mustard, S. L. Murchie, J.-P. Bibring, A. Meunier, A. A. Fraeman, and Y. Langevin, "Subsurface water and clay mineral formation during the early history of Mars," Nature **479**, 53–60 (2011).
41. S. L. Murchie, J. F. Mustard, B. L. Ehlmann, R. E. Milliken, J. L. Bishop, N. K. McKeown, E. Z. Noe Dobrea, F. P. Seelos, D. L. Buczkowski, S. M. Wiseman, R. E. Arvidson, J. J. Wray, G. Swayze, R. N. Clark, D. J. Des Marais, A. S. McEwen, and J.-P. Bibring, "A synthesis of Martian aqueous mineralogy after 1 Mars year of observations from the mars reconnaissance orbiter," J. Geophys. Res. **114**, 1–30 (2009).
42. J. Farmer and D. J. Des Marais, "Exploring for a record of ancient Martian life," J. Geophys. Res. **104**, 26977–26995 (1999).
43. J. F. Mustard, M. Adler, A. Allwood, D. S. Bass, D. W. Beaty, J. F. Bell III, W. B. Brinckerhoff, M. Carr, D. J. Des Marais, B. Drake, K. S. Edgett, J. Eigenbrode, L. T. Elkins-Tanton, J. A. Grant, S. M. Milkovich, D. Ming, C. Moore, S. Murchie, T. C. Onstott, S. W. Ruff, M. A. Sephton, A. Steele, and A. Treiman, *Appendices to the Report of the Mars 2020 Science Definition Team* (Mars Exploration Program Analysis Group, 2013), p. 154.
44. J. L. Bishop and E. Murad, "Characterization of minerals and biogeochemical markers on mars: a Raman and IR spectroscopic study of montmorillonite," J. Raman Spectrosc. **35**, 480–486 (2004).
45. D. D. Wynn-Williams and H. G. M. Edwards, "Proximal analysis of regolith habitats and protective biomolecules *in situ* by laser Raman spectroscopy: an overview of terrestrial Antarctic habitats and mars analogs," Icarus **144**, 486–503 (2000).
46. H. G. M. Edwards, I. B. Hutchinson, R. Ingley, J. Parnell, P. Vitek, and J. Jehlicka, "Raman spectroscopic analysis of geological and biogeological specimens of relevance to the ExoMars mission," Astrobiology **13**, 543–549 (2013).
47. J. Flahaut, J. Carter, F. Poulet, J.-P. Bibring, W. van Westrenen, G. R. Davies, and S. L. Murchie, "Embedded clays and sulfates in Meridiani Planum, Mars," Icarus **248**, 269–288 (2015).
48. A. Wang, J. F. Freeman, B. L. Joliff, and I.-M. Chou, "Sulfates on mars, a systematic Raman spectroscopic study of hydration states of magnesium sulfates," Geochem. Cosmochim. Acta **70**, 6118–6135 (2006).
49. C. Ross and S. Hendricks, "Minerals of the montmorillonite group: their origin and relation to soils and clays," in *Geological Survey Professional Paper 205-B* (U.S. Government Printing Office, 1945).
50. J. M. Alia, H. G. M. Edwards, F. J. Garcia-Navarro, J. Parras-Armenteros, and C. J. Sanchez-Jiminez, "Application of FT-Raman spectroscopy to quality control in brick clays firing process," Talanta **50**, 291–298 (1999).
51. R. L. Frost, "The structure of the kaolinite minerals–a FT-Raman study," Clay Miner. **32**, 65–77 (1997).
52. V. Kosarova, D. Hradil, I. Nemec, P. Bezdicka, and V. Kanicky, "Microanalysis of clay-based pigments in painted artworks by the means of Raman spectroscopy," J. Raman Spectrosc. **44**, 1570–1577 (2013).
53. A. I. Alajtal, H. G. M. Edwards, M. A. Elbagerma, and I. J. Scowen, "The effect of laser wavelength on the Raman spectra of phenanthrene, chrysene, and tetracene: implications for extraterrestrial detection of polyaromatic hydrocarbons," Spectrochim. Acta Part A **76**, 1–5 (2010).
54. R. N. Clark, J. M. Curchin, and J. W. Barnes, "Detection and mapping of hydrocarbon deposits on Titan," J. Geophys.Res. **115**, E10005 (2010).
55. I. Daniel and H. G. M. Edwards, "Raman spectroscopy in biogeology and astrobiology," in *EMU Notes in Mineralogy*, J. Dubessy, M.-C. Caumon, and F. Rull, eds., Vol. **12**, Applications of Raman Spectroscopy to Earth Sciences and Cultural Heritage (European Mineralogical Union, 2012), pp. 391–413.
56. R. Wiens, S. Maurice, B. Barraclough, M. Saccoccio, and W. Barkley, and 75 more of the ChemCam Team, "The ChemCam instrument suite on the Mars Science Laboratory (MSL) rover: body unit and combined system tests," Space Sci. Rev. **170**, 167–227 (2012).
57. A. Steinmetz, D. Nodop, J. Limpert, R. Hohmuth, W. Richter, and A. Tünnermann, "2 MHz repetition rate, 200 ps pulse duration from a monolithic, passively *Q*-switched microchip laser," Appl. Phys. B **97**, 317–320 (2009).
58. E. Mehner, A. Steinmann, R. Hegenbarth, H. Giessen, and B. Braun, "Stable MHz-repetition-rate passively *Q*-switched microchip laser frequency doubled by MgO:PPLN," Appl. Phys. B **112**, 231–239 (2013).
59. B. Bernard, E. Mehner, D. Kopf, H. Giessen, and B. Braun, "26 ps pulses from a passively *Q*-switched microchip laser," Proc. SPIE **8960**, 89601D (2014).
60. J. Blacksberg, E. Alerstam, Y. Maruyama, C. Cochrane, and G. R. Rossman, "Advances in time resolved Raman spectroscopy for *in situ* characterization of minerals and organics," Houston, Texas, Lunar and Planetary Institute, Lunar and Planetary Science XLVI, abstract 1304 (2015).